

The MHD Stability of Global Modes and Fast Particle Confinement in a Quasi-Axisymmetric Tokamak - Stellarator Hybrid

M. I. Mikhailov^{a, *}, J. Nührenberg^b, and R. Zille^c

Translated by E. Voronova

^a *Kurchatov Institute National Research Center, Moscow, 123182 Russia*

^b *Max-Planck-Institut für Plasmaphysik, Greifswald, D-17491 Germany*

^c *Max-Planck-Institut für Plasmaphysik, Garching, D-85748, Germany*

**e-mail: mikhaylov_mi@nrcki.ru*

Received May 17, 2019;

Revised May 23, 2019;

Accepted June 20, 2019

Abstract—The compatibility of global MHD modes and good collisionless confinement of fast particles is studied in a quasi-axisymmetric tokamak - stellarator hybrid. It is shown that both of these requirements can be satisfied at a relative plasma pressure up to $\langle \beta \rangle \sim 0.02$.

1. INTRODUCTION

A quasi-axisymmetric tokamak, i.e., a stellarator with a toroidal current, was proposed in [1]. In this work, we consider a two-period configuration with an aspect ratio $A \sim 4$, in which the stellarator rotational transform was $\iota(0) = 0.1$ at the axis and $\iota(1) = 0.14$ at the plasma boundary (the corresponding values at a single period of the magnetic field were of 0.05 and 0.07, respectively). The total rotational transform was set as $\iota = 0.91 - 0.59s$, where s is the normalized toroidal flux. This transform was obtained by creating a suitable distribution of the toroidal current. In this configuration, the collisionless confinement of α particles at reactor

parameters (magnetic field $B = 5$ T and installation volume $V = 1000$ m³) was very good (almost all particles launched at one-half of the minor radius were confined during 1 second). In [1], the stability of the global MHD modes was not considered.

Since the concept of axial quasi-symmetry is attractive due to the potential ability of such machines to operate without disruptions [2], in this work, we analyze the MHD stability of the quasi-axisymmetric tokamak and stellarator hybrid with a good confinement of fast particles in more detail than in [3].

2. OPTIMIZATION TOWARD QUASI-AXISYMMETRY

The condition of axial quasi-symmetry, which translates into the absence of Fourier harmonics B_{mn} with $n \neq 0$ in the module of the magnetic field in the magnetic coordinates, can be easily used to optimize our configuration to quasi-symmetry. It was stated in [4] and shown more strictly in [5, 6] that the quasi-symmetry condition cannot be strictly satisfied in the entire volume of the plasma column. In this case, the use of different penalty functions to achieve quasi-symmetry can lead to slightly different results. Examples of the correction functions are, e.g., a sum of the absolute values of harmonics B_{mn} that break the symmetry, or the sum of the squares of their values. These sums can be calculated over a set of magnetic surface or over the entire volume of the plasma column. We note that for optimization, the stellarator rotational transform is to be considered as an external parameter; therefore, it has to be determined using additional considerations.

In [7], it was shown that a one-dimensional spectrum of the magnetic field B (in addition to its dependence on the flux coordinate) provides the conservation of the additional integral of the drift equations of motion, the same as in truly symmetrical configurations. This means that in the magnetic coordinates, the shape of the banana trajectory is independent of the longitudinal coordinate. From the viewpoint of particle confinement, the less strict condition of the constancy of the second adiabatic invariant J_{\parallel} at the magnetic surface (the center of the banana trajectory of a trapped particle moves along the magnetic surface) can be used for

optimization together with the condition of pseudo-symmetry [8]. If this condition is satisfied, there are no islands on the map of the lines $B = \text{const}$ at the magnetic surfaces and no locally trapped particles. This condition can also be expressed as the module of the magnetic field being two-dimensional in some flux coordinates with straight magnetic field lines. In the near-axial approximation, the condition of quasi-symmetry and the condition $J_{\parallel} = J_{\parallel}(s)$ for all trapped particles are the same, while further along the radius they begin to differ. For good particle confinement, one can use an even softer condition that for all values of $B_{reflect}$ (i.e., for all trapped particles), the contours of the second adiabatic invariant for the particles launched from a set magnetic surface do not exceed the boundary of the plasma column. This condition, together with the pseudo-symmetry and quasi-axisymmetry conditions, was used in this work. In a similar manner to [1], we consider a two-period configuration with an aspect ratio $A \sim 4$.

Figure 1 shows the cross sections of the magnetic surfaces in the configuration found at $\langle \beta \rangle = 0.019$ and the radial profiles of the rotational transform, the magnetic well, and the plasma pressure, which is flattened near the $2/3$ and $1/2$ resonances. The pressure and longitudinal current density profiles were assumed to have the shapes $p \sim (1 - s)^2$ and $j \sim 0.1(1 - s^2)^3 + 0.9(1 - s)^3$, respectively. The rotational transform near the magnetic axis is close to unity (0.97), the $\iota = 1/2$ resonant surface is located inside the plasma column, and $\iota(1) = 0.44$. At the determined boundary magnetic surface, the rotational transform of the vacuum magnetic field is 0.27 near the magnetic axis and 0.31 near the boundary. The effective ripple ($\epsilon^{3/2}$) varies from 6×10^{-5} near the magnetic axis to 2×10^{-4} near the boundary. The fast particle confinement is very good. At the reactor parameters mentioned above, out of 1000 α particles launched from one-half of the minor radius, 280 particles are reflected and only a few (~ 5) particles escape the plasma during 1 s. The fast-particle confinement and effective ripple depend weakly on plasma pressure, but they are sensitive to the longitudinal current: at a fixed current profile, decreasing the longitudinal current at first (at $\iota(0) \sim 0.77$) weakly affects the fast-particle confinement (0–10 particles escape), but at $\iota(0) <$

0.72 the losses grow rapidly and at $\iota(0) = 0.58$ they reach up to one-third of the number of reflected particles.

3. THE STABILITY OF THE GLOBAL MHD MODES

The stability of the ideal global MHD modes was studied using the CAS3D computer code [9]. We considered modes with a free boundary [10], there was no conducting case, and the normalization was made with respect to the component of the perturbed magnetic field transverse to the magnetic surface. In the two-period configuration, two independent mode families can be separated, modes with toroidal indices $n = -1 + 2k$ (first family) and $n = 2k$ (second family), where k is an integer. The number of points along the minor radius was 576, the maximum poloidal index m was 15, and the total number of Fourier modes was approximately 100. These parameters allowed us to consider three types of modes, the internal kink modes with small m numbers, the ballooning modes, and the peeling modes [11]. The latter two mode types have larger m numbers. In all mode analyses, the equilibrium boundary magnetic surface, the equilibrium current density profile, and total longitudinal current were constant. We considered several values of the equilibrium plasma pressure.

a) Internal kink modes

At the value of the total longitudinal current under study here, there are two resonant magnetic surfaces with low m numbers inside the plasma column: $\iota = 2/3$ and $\iota = 1/2$. The corresponding resonant modes belong to different families and should be considered separately. For the first family, Fig. 2 shows the radial profile of the ten largest Fourier harmonics of the radial displacement at a relative pressure $\langle\beta\rangle = 0.019$. Although the contribution from the plasma region to the perturbation energy is negative, $W_p = -0.135$, the positive contribution of the vacuum region, $W_{vac} = 0.138$, makes the mode stable: $\lambda = W_p + W_{vac} = 0.003$. It is seen that in the global mode considered, besides the connection between the modes with equal n numbers, characteristic of a tokamak, the connection between the modes with different n numbers that are characteristic of a stellarator is also present. Since the

number of periods is small ($N = 2$), the rational surfaces with $\iota = n/m$ with different n numbers and close m numbers are inside the plasma column. For harmonics with resonant surface inside the plasma column, the maximum amplitudes of the radial component of the displacement are reached near the corresponding resonant surfaces. Figure 3 shows the radial distributions of the different depositions into $W_p = \int d\tau [|\mathbf{C}|^2 - A(\xi \cdot s)^2 + \gamma p (\nabla \cdot \xi)^2]$ (in detail, see [9]).

It is seen in Fig. 2 that the free boundary condition is substantial for the studied global mode, since many of its harmonics are finite at the boundary. At the same time, each of the terms that constitute W_p and W_p itself are small outside the magnetic surface with $\iota = 1/2$.

The corresponding mode from the second family with the maximum amplitudes of the Fourier harmonics with $m = 3, n = -2$ and $m = 4, n = -2$ is even more stable at $\langle \beta \rangle = 0.019$ (see Fig. 4). Here, the contribution of energy from the plasma region is positive $W_p = 0.103$, similar to the contribution of the vacuum region $W_{vac} = 0.045$, and $\lambda = 0.148$. The contributions to W_p decrease strongly outside of the resonant surface $\iota = 2/3$ (see Fig. 5). Comparison of the two global modes shows that the mode from the first family is marginally stable, while the mode from the second family is profoundly stable.

When the plasma $\langle \beta \rangle$ is increased, the mode from the first family becomes unstable. Figure 6 shows a spectrum of the unstable mode with the main harmonic $m = 2, n = -1$ at $\langle \beta \rangle = 0.024$. Here, $W_p = -0.189$ and $W_{vac} = 0.158$, so that $\lambda = -0.031$. At this plasma pressure, the mode from the second family continues to be stable. Figure 7 shows a weakly unstable mode from the second family at $\langle \beta \rangle = 0.029$. For this mode, $W_p = -0.087$ and $W_{vac} = 0.073$, so that $\lambda = -0.014$.

Comparison of these results shows that the limit of the plasma pressure for internal kink modes is $\langle \beta \rangle = 0.02$.

b) Ballooning modes

The studied modes allow us to consider modes with higher m and n numbers (ballooning modes). These are also considered as modes with a free boundary.

Figure 8 shows the radial profiles of the harmonics of the normal displacement at $\langle\beta\rangle = 0.019$. This is a mode from the first family, which is profoundly stable: $W_p = 0.011$ and $w_{vac} = 0.014$, so that $\lambda = 0.025$. This mode can be considered as transient between the internal kink mode and the ballooning mode. Modes whose structures are even closer to ballooning are even more stable. When the plasma pressure is increased sufficiently, the ballooning modes become unstable. Figure 9 shows an example of unstable ballooning modes at $\langle\beta\rangle = 0.024$. Here, $W_p = -0.093$ and $w_{vac} = 0.006$, $\lambda = -0.087$, and the deposition of the vacuum region is one order of magnitude smaller than the contribution of the plasma region. It can be said that the pressure limit for the stability of ballooning modes is higher than the pressure limit of the internal kink modes.

c) Peeling modes

For the profiles studied, the plasma pressure and the longitudinal current density become zero near the plasma column boundary. At the initial plasma pressure ($\langle\beta\rangle = 0.019$), no unstable peeling modes are observed. They appear when the pressure is increased: at $\langle\beta\rangle = 0.024$, $\lambda = -0.079$ ($W_p = -0.108$ and $w_{vac} = 0.029$, see Fig. 10). When the pressure is increased further, $\langle\beta\rangle = 0.029$, the mode gets more unstable: $\lambda = -0.162$ ($W_p = -0.196$ and $w_{vac} = 0.034$, see Fig. 11). In both cases, the mode whose resonant magnetic surface is close to the plasma boundary is the mode with $m = 7$, $n = -3$, and $\iota_{res} = 0.43$, whose resonant magnetic surface is outside the plasma column boundary (at $\langle\beta\rangle = 0.024$, $\iota(1) = 0.442$ and at $\langle\beta\rangle = 0.029$, $\iota(1) = 0.444$). An interpolation of these results allows us to conclude that the initial configuration with $\langle\beta\rangle = 0.019$ is marginally stable with respect to the peeling modes.

4. DISCUSSION OF RESULTS

It follows from previous works (see, e.g., [1, 3, 12, 13]) that achieving a low effective ripple in a quasi-axisymmetric configuration is not problematic. In this

work, similar to [3], it is shown that in quasi-axisymmetric configurations, low effective ripple and good collisionless confinement of fast particles at reactor parameters can be achieved simultaneously. In this work, at fixed plasma pressure and longitudinal current density profiles, a good particle confinement is realized in both the initial configuration with $\iota(0) = 0.96$ and at a lower longitudinal current, down to $\iota(0) = 0.77$. However, further decrease of the longitudinal current leads to an increase in the loss of trapped particles, and at $\iota(0) = 0.58$, approximately one-third of the trapped particles are lost during 1 s. Accordingly, in this work, the stability of the global modes is studied in a quasi-axisymmetric configuration with a strong longitudinal current. It is shown above that in this $N = 2$ quasi-axisymmetric configuration with $\iota(0)$ close to unity, the maximum stable plasma pressure is $\langle\beta\rangle = 0.02$ for the studied pressure and current density profiles. At larger $\langle\beta\rangle$, the peeling modes and internal kink modes, followed by ballooning modes, become unstable. As shown in this work, a good confinement of fast particles can be achieved at somewhat lower values of the longitudinal current. The stability of the global modes in these configurations should be studied further for equilibria with different boundaries.

FUNDING

This work was carried out for the Eurofusion consortium. It was supported by the Euratom research and training Work Program for 2014–2018 and 2019–2020 under Agreement no. 633053. The reasoning and opinions presented in this work do not necessarily reflect the position of the European commission.

ACKNOWLEDGMENTS

We are grateful to Professors S. Günter and P. Helander for their support. We thank Carolin Nührenberg for technical help with using the CAS3D code.

REFERENCES

1. J. Nührenberg, W. Lotz, and S. Gori, in *Proceedings of the Joint Varenna–Lausanne International Workshop on Theory of Fusion Plasmas, Varenna, 1994*, Ed. by E. Sindoni and J. Vaclavik (Compositori, Bologna, 1994), p. 3.
2. D. A. Maurer, S. F. Knowlton, J. D. Hanson, G. J. Hartwell, M. C. Miller, B. A. Stevenson, X. Ma, J. Herfindal, and M. Pandya, in *Proceedings of the 39th EPS Conference on Plasma Physics, Stockholm, 2012*, ECA **36F**, P-2.065 (2012).
<http://ocs.ciemat.es/epsicpp2012pap/pdf/P2.065.pdf>.
3. S. A. Henneberg, M. Drevlak, C. Nührenberg, C. D. Beidler, Y. Turkin, J. Loizu, and P. Helander, *Nucl. Fusion* **59**, 026014 (2019).
4. D. A. Garren and A. H. Boozer, *Phys. Fluids B* **3**, 2822 (1999).
5. G.G. Plunk and P. Helander, *J. Plasma Phys.* **84**, 905840205 (2018).
6. M. Landreman, W. Sengupta, and G.G. Plunk, *J. Plasma Phys.* **85**, 905850103 (2019).
7. A. H. Boozer, *Phys. Fluids* **26**, 496 (1983).
8. M. I. Mikhailov, V. D. Shafranov, and D. Sunder, *Plasma Phys. Rep.* **24**, 653 (1998).
9. C. Schwab, *Phys. Fluids B* **5**, 3195 (1993).
10. P. Merkel, C. Nührenberg, and W. A. Cooper, in *Proceedings of the ISPP-17 Joint Varenna–Lausanne International Workshop on Theory of Fusion Plasmas, Varenna, 1996*, Ed. by J. W. Connor, E. Sindoni, and J. Vaclavik (Societa Italiana de Fisica, Bologna, 1996), p. 233.
11. D. Lortz, *Nuclear Fusion* **15**, 49 (1975).
12. J. Nührenberg, R Zille, S Okamura, K. Matsuoka, and S Murakami, *Plasma Phys. Contr. Fusion* **43**, 137 (2001).
13. B.E. Nelson, L.A. Berry, A.B. Brooks, M. J. Cole, J. C. Chrzanowski, H.-M. Fan, P. J. Fogarty, P. L. Goranson, P. J. Heitzenroeder, S. P. Hirshman, G. H. Jones, J. F. Lyon, G. H. Neilson, W. T. Reiersen, D. J. Strickler, et al, *Fusion Eng. Des.* **66**, 169 (2003).

FIGURE CAPTIONS

Fig. 1. Transverse cross sections (start, quarter- and half-period) in an $N = 2$ configuration with longitudinal current optimized to quasi-axisymmetry at $\langle \beta \rangle = 0.019$ (top) and radial profiles of the rotational transform, magnetic well, and plasma pressure (bottom).

Fig. 2. The profiles of the ten largest Fourier harmonics of the radial component of the displacement in the initial configuration with $\langle\beta\rangle = 0.019$, the first family.

Fig. 3. Contributions to the integral energy perturbation averaged over magnetic surfaces as functions of the normalized toroidal flux for the initial configuration; (1) C^1 is caused by the curvature of the magnetic field lines, (2) C^2 is expressed through the local shear and the parallel current density, (3) C^3 is mainly caused by the variation of the longitudinal field, (4) C^4 is the potentially destabilizing term $A(\xi \cdot \nabla s)^2$, C^5 is the term caused by plasma compression, and (6) C^6 is W_p .

Depositions 3 and 4 are small and not shown in this figure.

Fig. 4. The same as in Fig. 2 for the second family.

Fig. 5. The same as in Fig. 2 for the second family.

Fig. 6. The profiles of the ten largest Fourier harmonics of the radial component of the displacement at $\langle\beta\rangle = 0.024$, the first family. This mode is unstable.

Fig. 7. The profiles of the ten largest Fourier harmonics of the radial component of the displacement at $\langle\beta\rangle = 0.029$, the second family. This mode is unstable.

Fig. 8. The Fourier harmonics of the radial component of the displacement for a ballooning-type perturbation, the first family, at $\langle\beta\rangle = 0.019$. This mode is stable.

Fig. 9. The same as in Fig. 8 at $\langle\beta\rangle = 0.024$, the first family. This mode is unstable.

Fig. 10. The Fourier harmonics of the radial component of the displacement for the peeling mode, the first family at $\langle\beta\rangle = 0.024$. This mode is unstable.

Fig. 11. The same as in Fig. 10 at $\langle\beta\rangle = 0.029$. This mode is unstable.

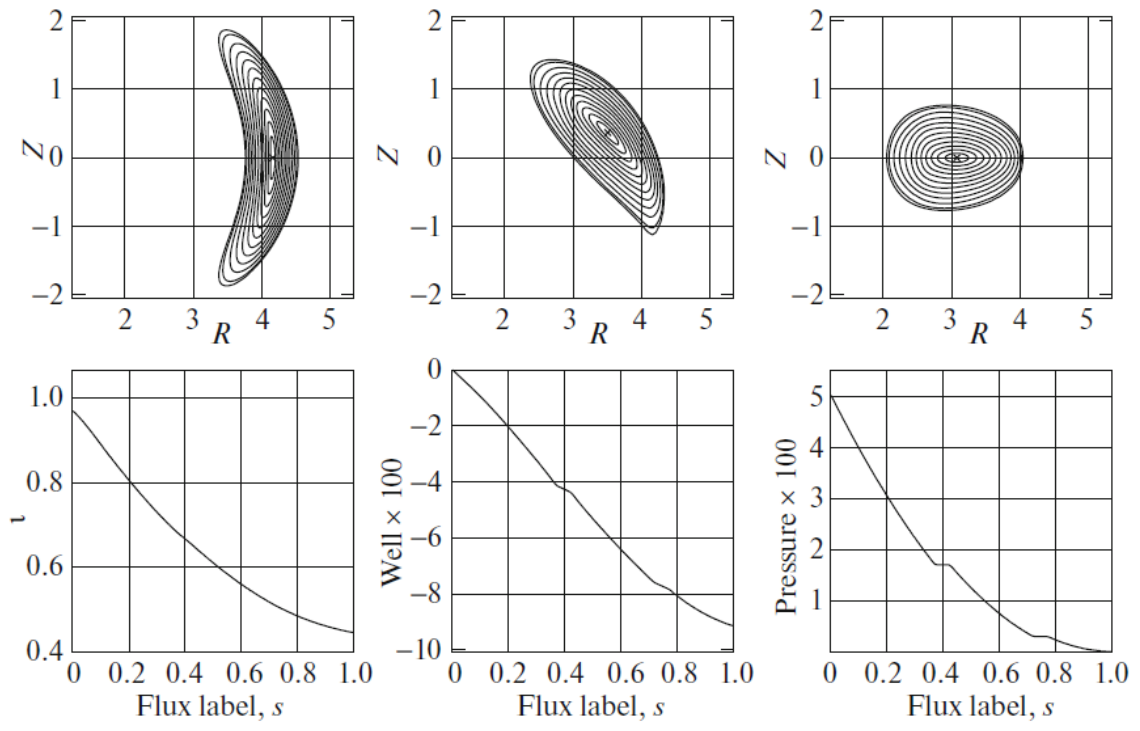


Fig.1

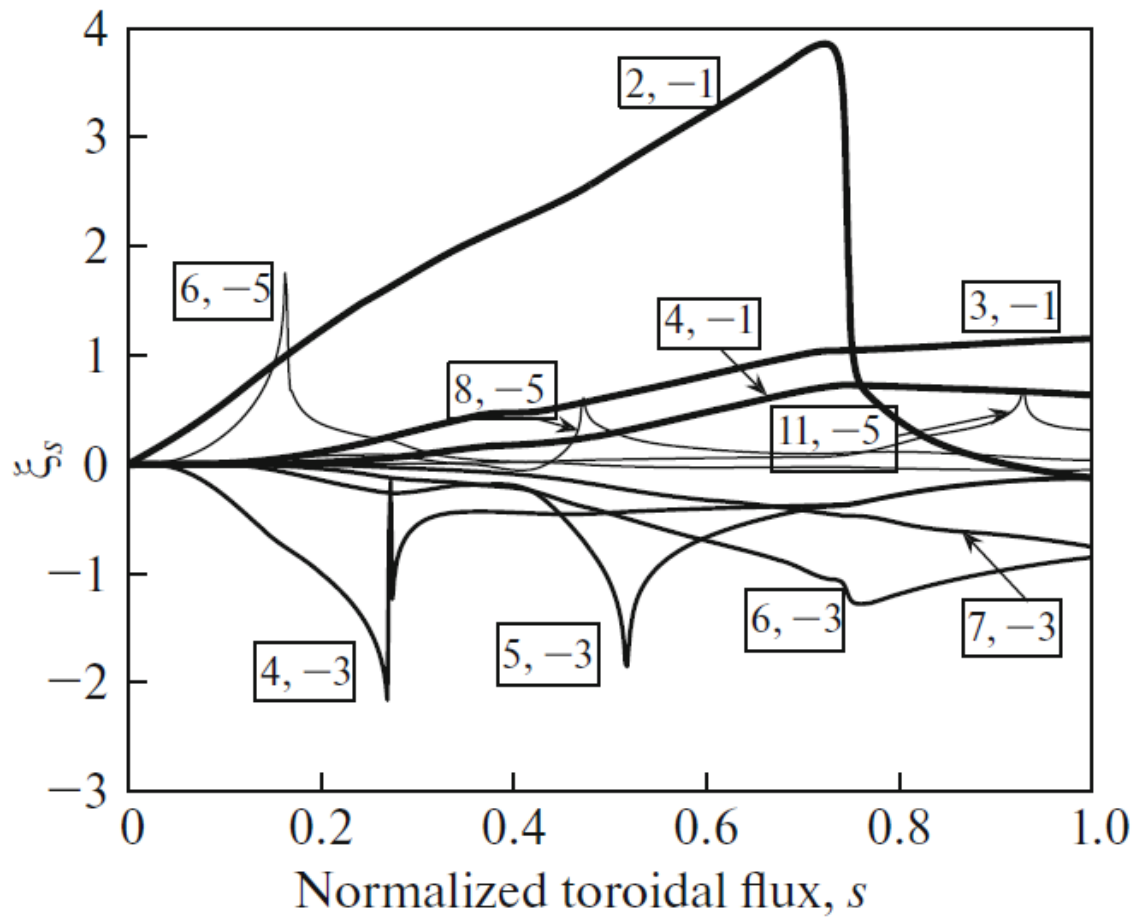


Fig.2

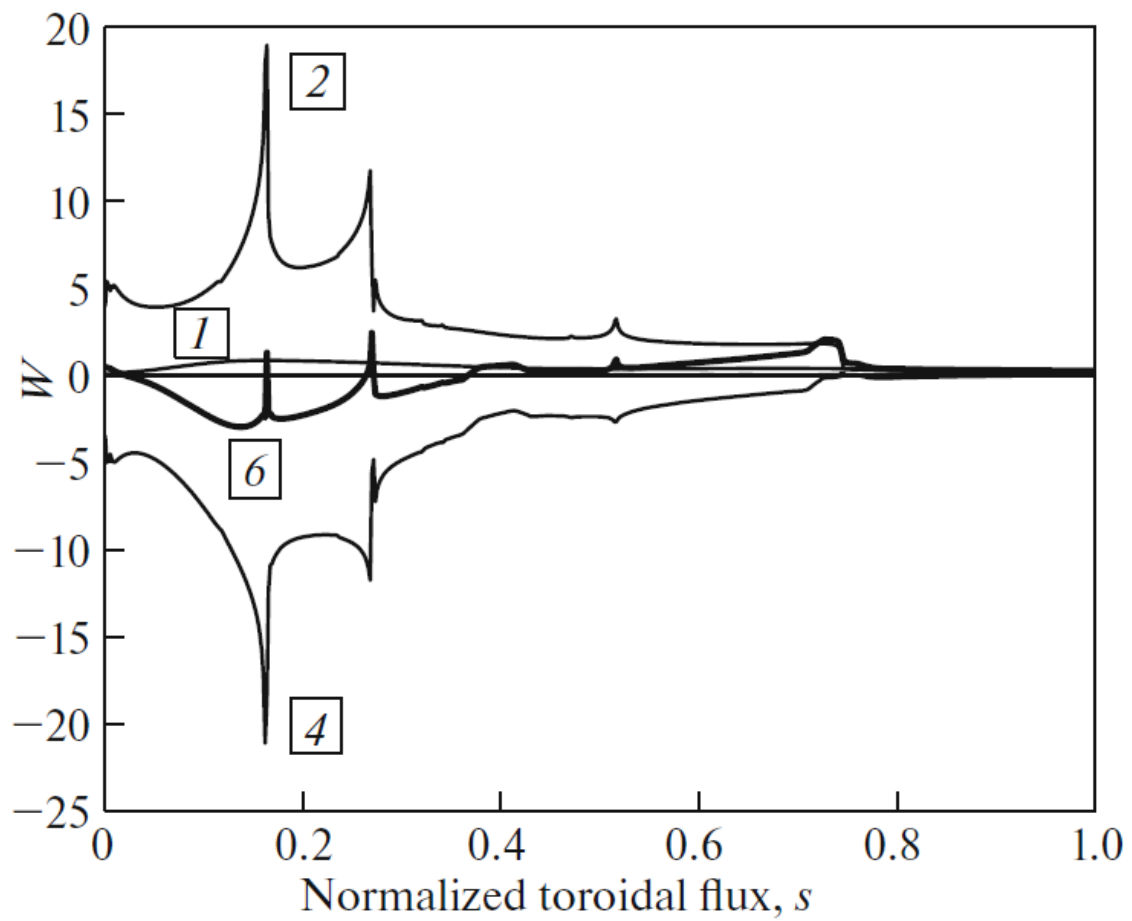


Fig.3

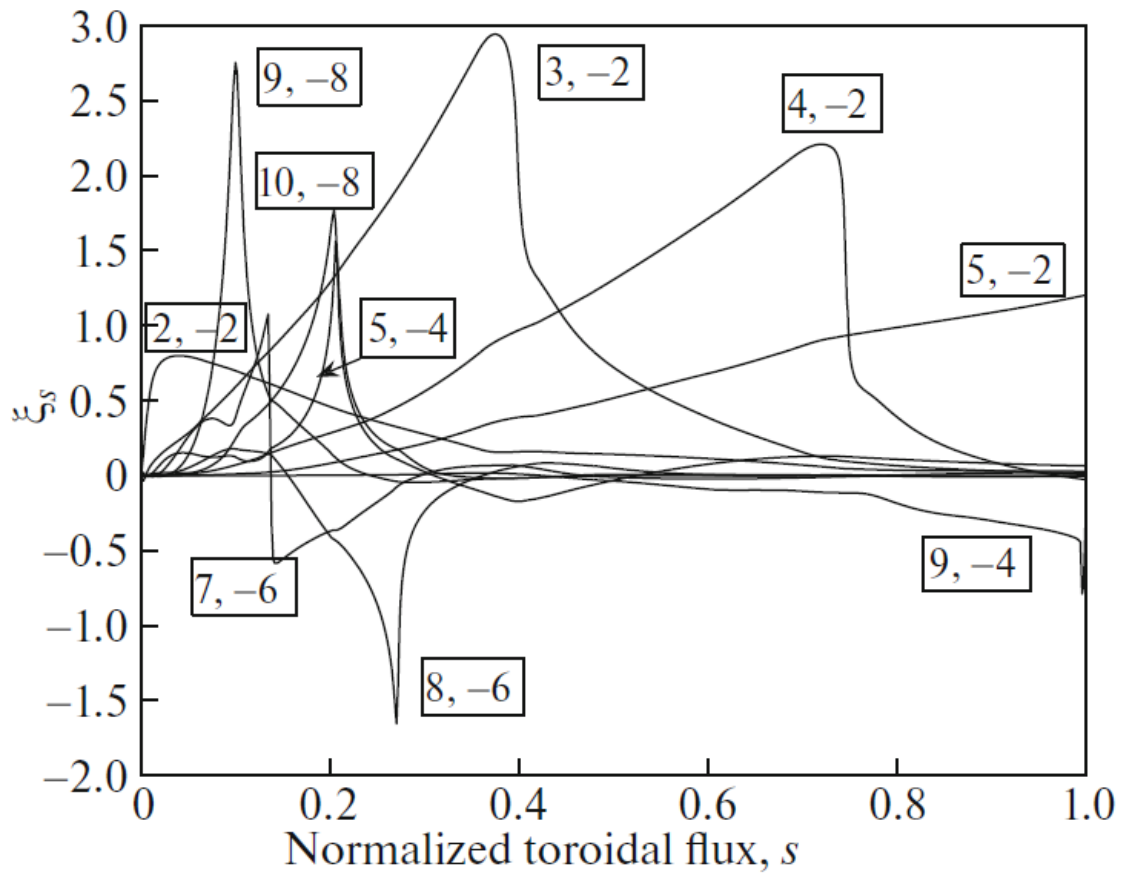


Fig.4

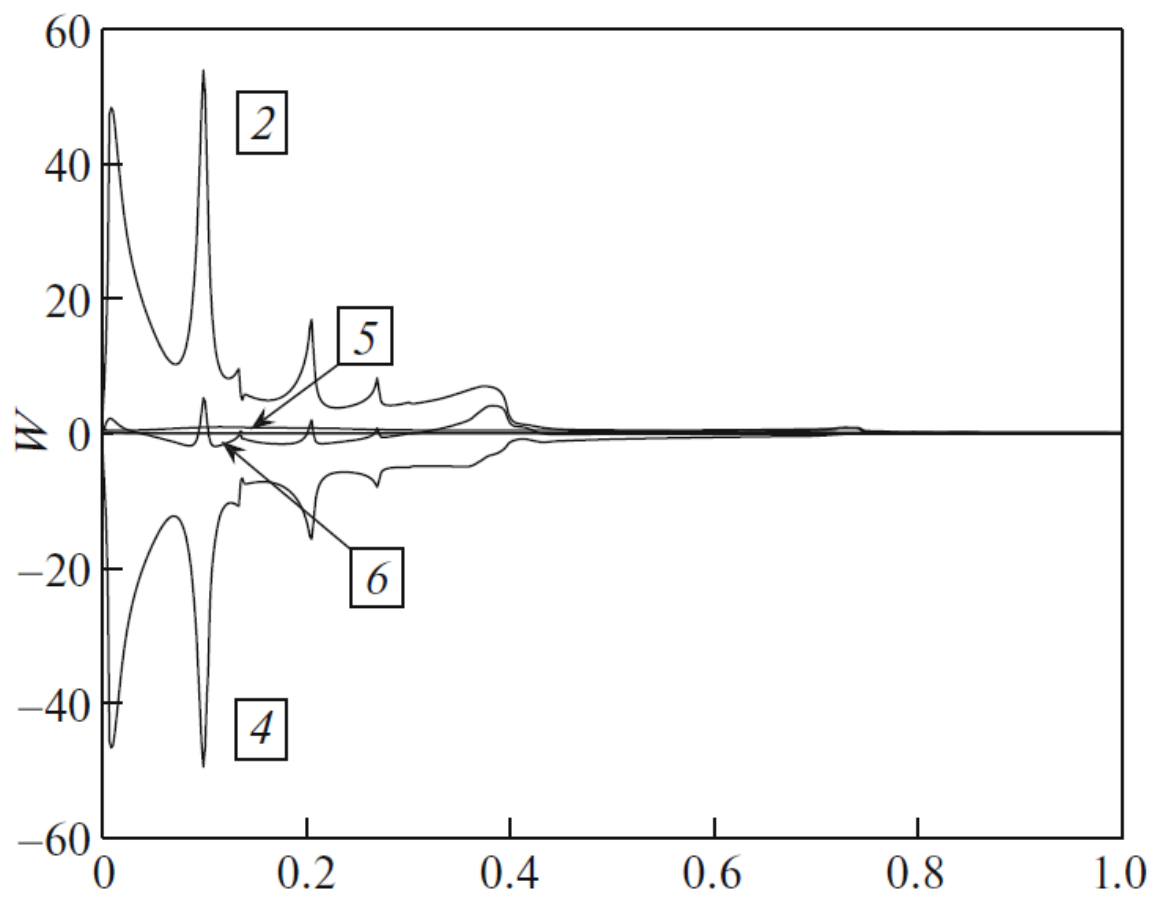


Fig.5

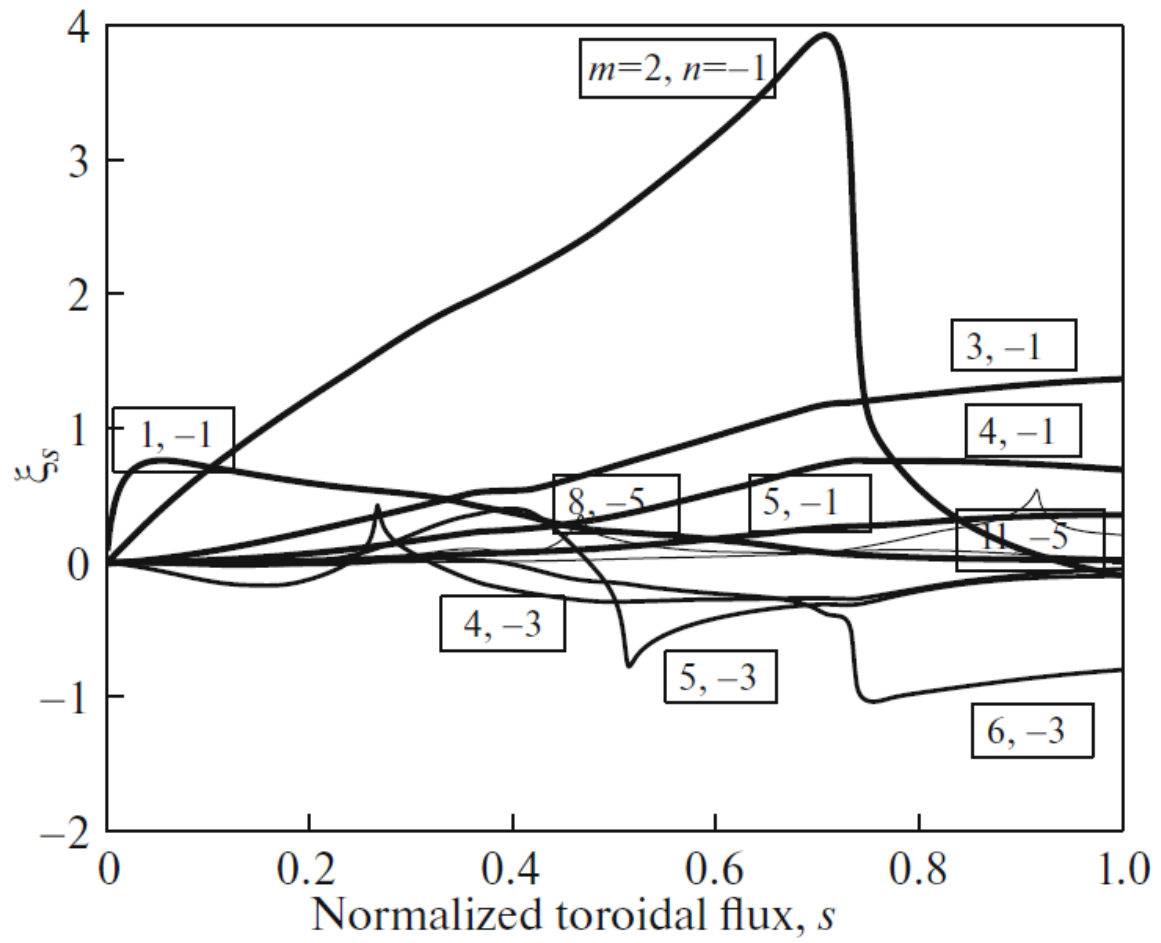


Fig.6

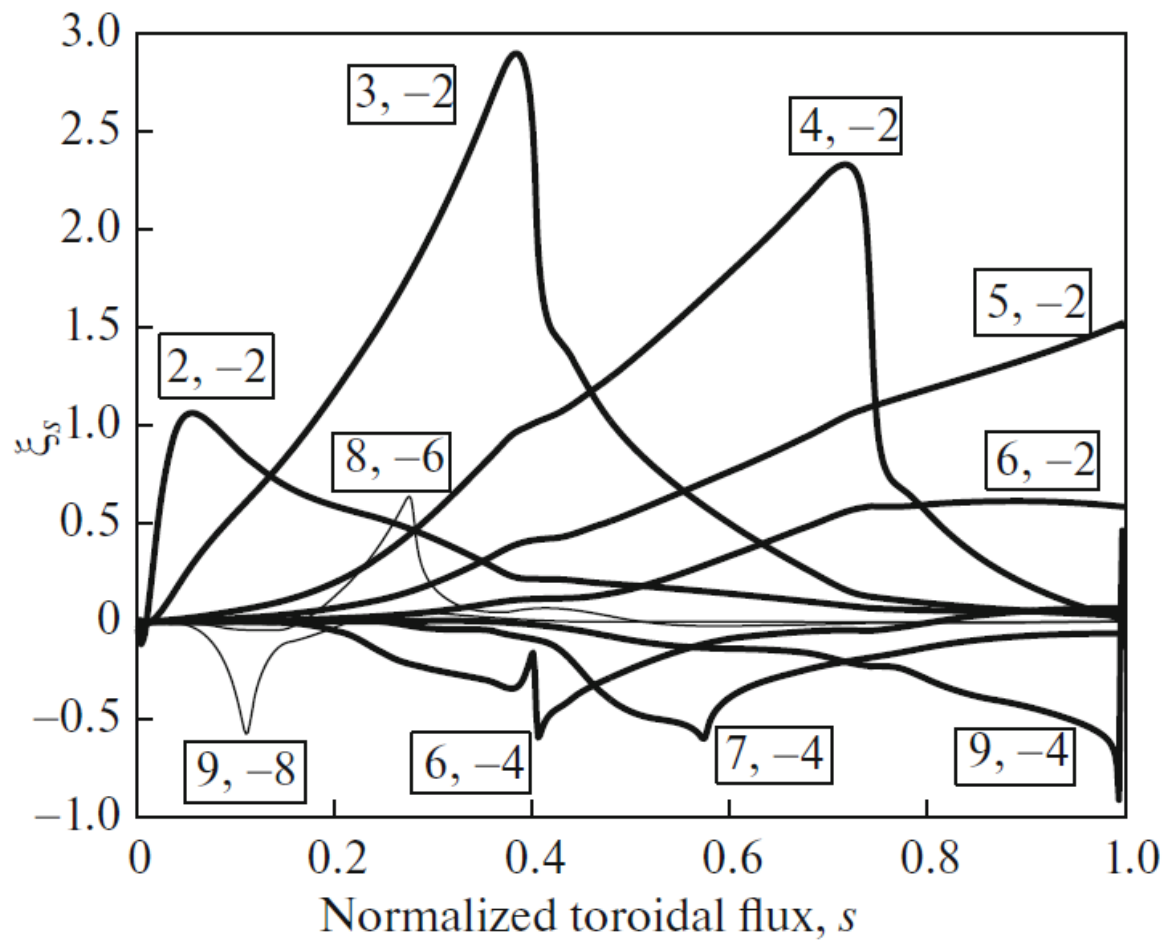


Fig.7

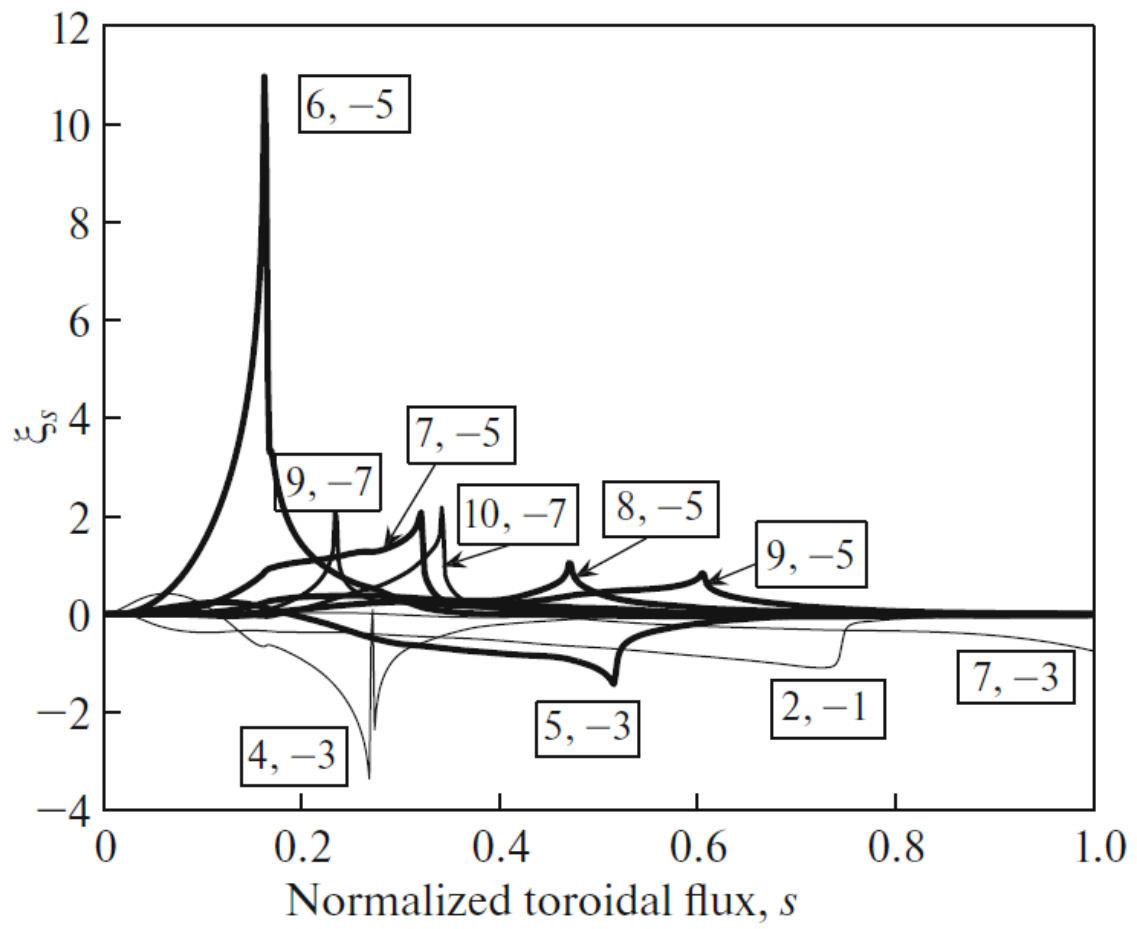


Fig.8

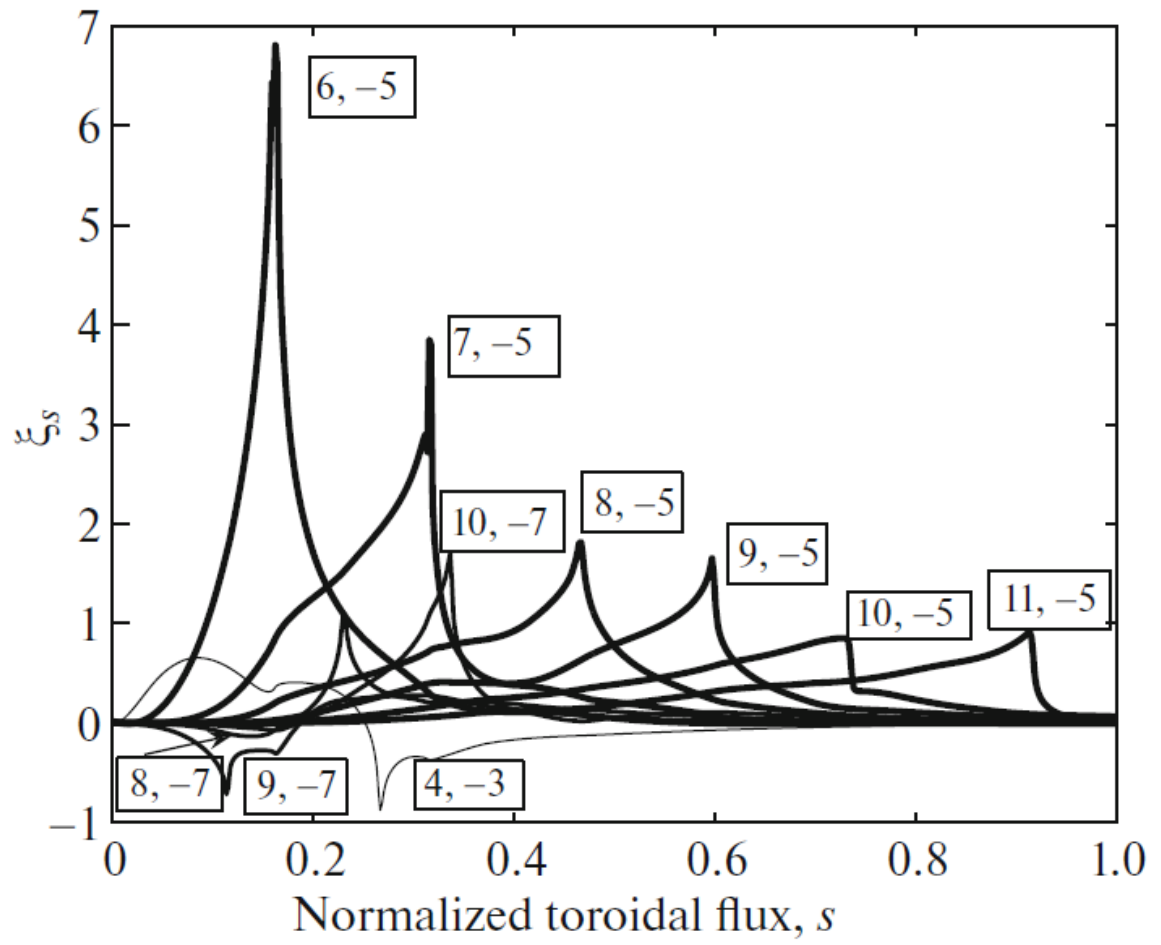


Fig.9

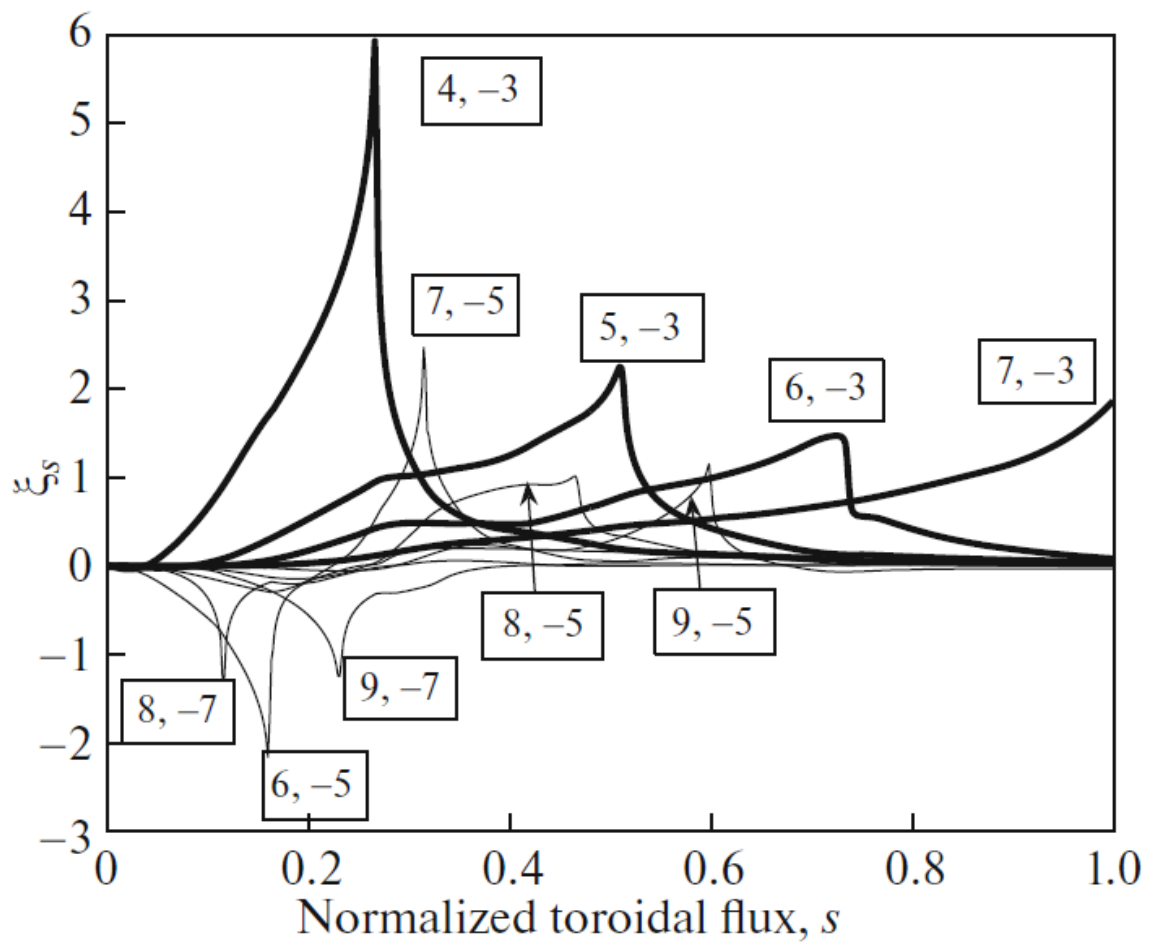


Fig.10

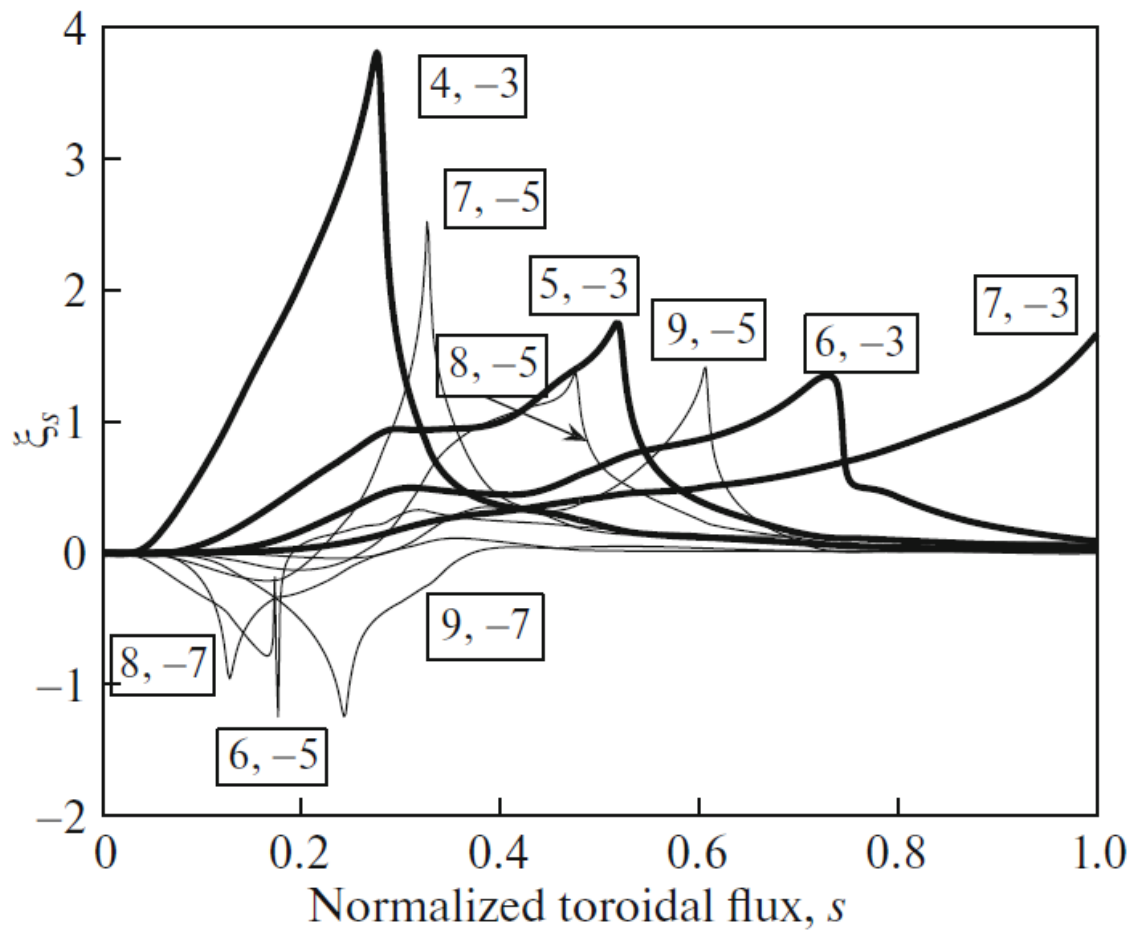


Fig.11